CHAPTER 4: PREPARATION AND CHARACTERIZATION OF Pt(POP-BF$_2$)$^{5-}$ AND Pt(POP-BF$_2$)$^{6-}$

Extensive studies of Pt(pop)$^{4-}$ have demonstrated that optical excitation of an electron populates a pσ orbital with bonding character[1], which strengthens the Pt-Pt interaction and causes a shortening of the Pt-Pt distance by 0.21-0.31 Å as determined by both X-ray and optical techniques.[2-4] Theoretical work performed by Lam in collaboration with Vlček and Záliš predicted an analogous bond shortening of 0.18 Å in Pt(pop-BF$_2$)$^{4-}$.[5] As in optical excitation, direct reduction of Pt(pop-BF$_2$)$^{4-}$ was expected to fill the pσ orbital, forming a weak Pt-Pt bond. While reversible electrochemical reduction of the parent compound Pt(pop)$^{4-}$ has never been reported, Pt(pop)$^{5-}$ has nevertheless been generated via pulse radiolysis in aqueous solution.[6,7] Given the lack of easily reduced –O—H···O— groups in Pt(pop-BF$_2$)$^{4-}$, reversible reduction seemed likely, and electrochemical studies were undertaken.

4.1   Electrochemical reductions

Pt(pop-BF$_2$)$^{4-}$ in acetonitrile (MeCN) undergoes one-electron reductions at $E_{1/2}$ = -1.68 V and E_P = -2.46 V vs Fc$^+$/Fc (Figure 1).[i] The first wave is chemically reversible and electrochemically quasireversible at a scan rate of 50 mV/s, as shown by the ΔE_p = 155 mV for the wave of interest vs ~100 mV for Fc$^+$/Fc under very similar conditions. The second wave is electrochemically irreversible and chemically reversible, indicating formation of a superreduced complex Pt(pop-BF$_2$)$^{6-}$ which is stable at least at 273 K (see 4.2). Scanning anodically, a 2-electron chemically

---

[i] Electro- and spectroelectrochemical data were collected in collaboration with Bryan M. Hunter and Michael G. Hill.

irreversible oxidation is observed at +0.94 V vs Fc⁺/Fc. The full-range cyclic voltammogram is shown in Figure 2.
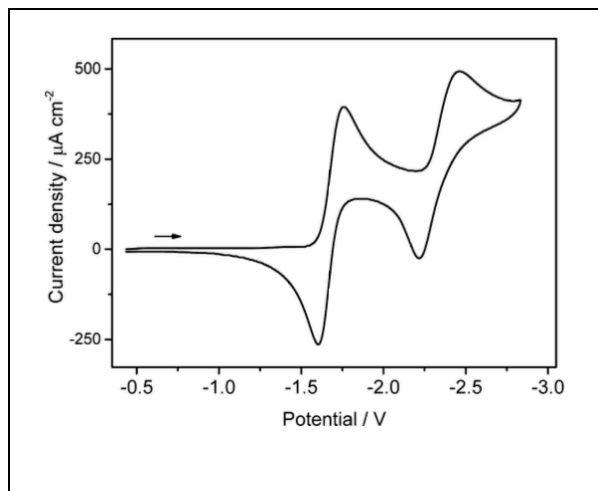
Figure 1: Cyclic voltammogram of Pt(pop-BF$_2$)$^{4-}$ in MeCN containing 0.1 M tetrabutylammonium hexafluorophosphate (Bu$_4$NPF$_6$) at 273 K. Potentials vs Fc⁺/Fc; scan rate of 50 mV/s.	Figure 2: Full-range cyclic voltammogram of Pt(pop-BF2)4- in MeCN containing 0.1 M (Bu4NPF6) at 273 K. Potentials vs Fc+/Fc; scan rate of 200 mV/s.
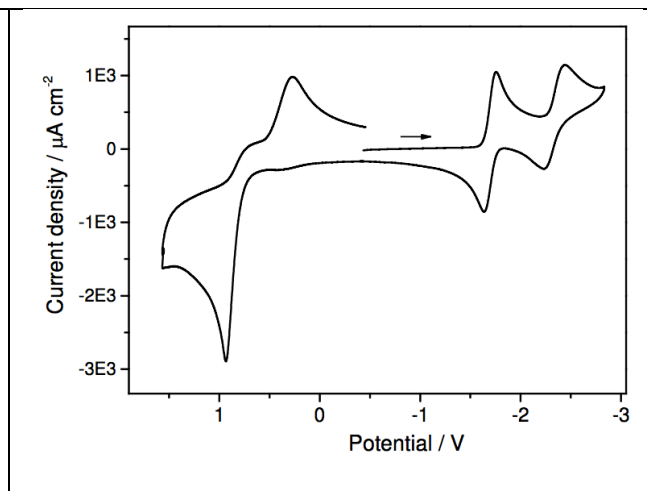
The first reduction of Pt(pop)$^{4-}$ has been estimated from reductive quenching kinetics to be approximately -1.8 V, as compared to the -1.68 V obtained for Pt(pop-BF$_2$)$^{4-}$.[8] This difference in potentials is likely attributable to the strong electron-withdrawing effects of the BF$_2$ groups, which may be transmitted to the metal atoms by delocalization of the pσ orbital over the phosphorous atoms acting as donors to the Pt-Pt unit.[9]

Furthermore, potentials for the excited state redox couples can be estimated at 1.57 V for ¹[Pt(pop-BF$_2$)$^{4-/5-}$]* and 0.86 V for ³[Pt(pop-BF$_2$)$^{4-/5-}$]* (both versus Fc⁺/Fc) using spectroscopically determined excited-state energies;[10] continuation of the work described in Chapter 3 could offer further insight into these values.

4.2   Optical properties

UV-Vis spectroelectrochemistry in acetonitrile at 273 K carried out at the potential of the first reduction showed a sharp decrease in intensity of the characteristic 365 nm absorption band of Pt(pop-BF$_2$)$^{4-}$. This decrease was accompanied by the rise of a sharp band at 416 nm with shoulders at ~411 nm and 450 nm, as well as broad weak bands at ~550 and 338
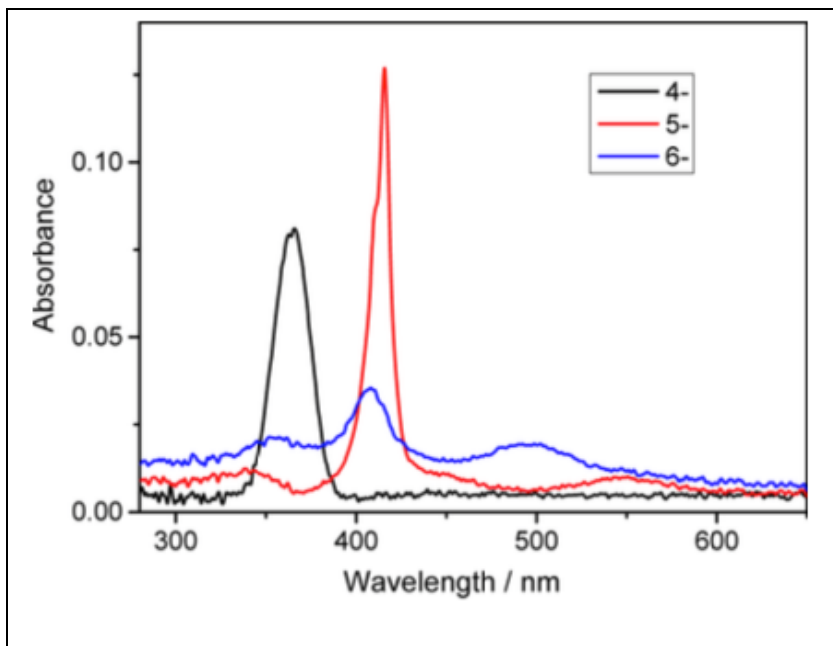
Figure 3: UV-Vis absorption spectra of Pt(pop-BF$_2$)$^{4-}$ (black) and in situ spectroelectrochemically produced Pt(pop-BF$_2$)$^{5-}$ and Pt(pop-BF$_2$)$^{6-}$ (blue; contains ~20% of Pt(pop-BF$_2$)$^{5-}$).

nm. All of these bands are attributable to Pt(pop-BF$_2$)$^{5-}$ (Figure 3). Upon anodically switching the
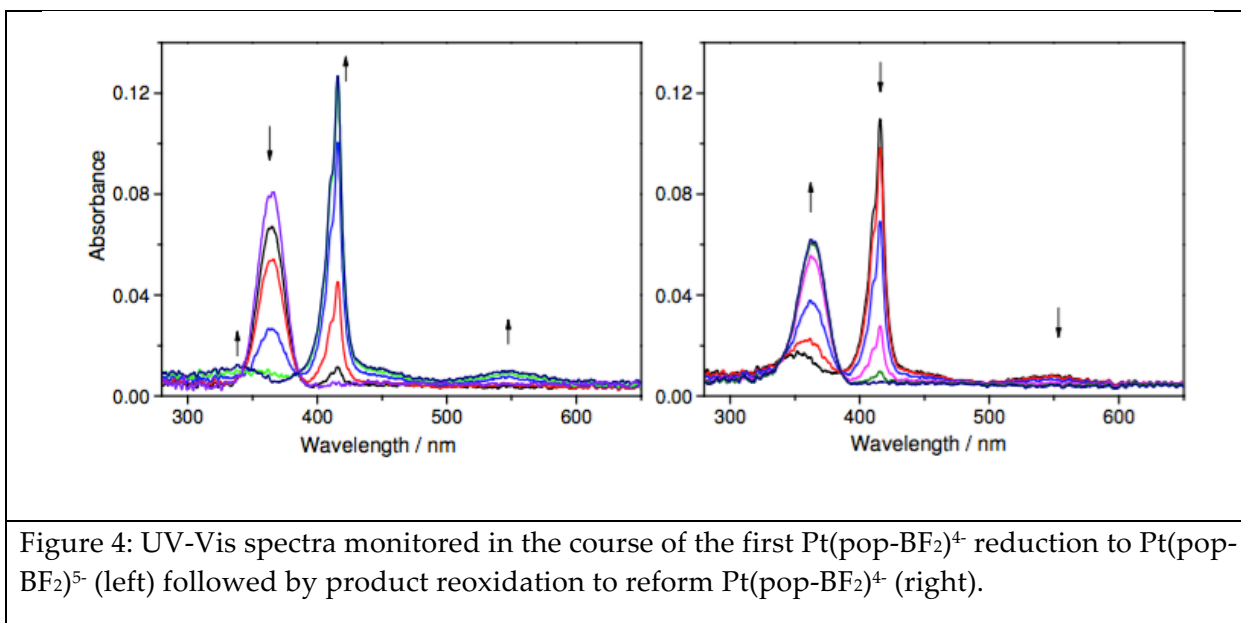
Figure 4: UV-Vis spectra monitored in the course of the first Pt(pop-BF$_2$)$^{4-}$ reduction to Pt(pop-BF$_2$)$^{5-}$ (left) followed by product reoxidation to reform Pt(pop-BF$_2$)$^{4-}$ (right).

potential, the parent complex Pt(pop-BF$_2$)$^{4-}$ is nearly quantitatively recovered (Figure 4). Further

reduction at more negative potentials yields a spectrum with distinct features at 356, 408, and 496

nm. Spectra measured during the second reduction indicate an isosbestic point, pointing to

conversion to the "superreduced" species Pt(pop-BF$_2$)$^{6-}$ (Figure 5). At low temperature (273 K),

reoxidation of this species eventually recovered Pt(pop-BF$_2$)$^{5-}$, while at room temperature a

different, unidentified species absorbing at 350 nm is formed upon reoxidation. In both Figure 4

and Figure 5, the slight decrease in absorption intensity upon recovery of the oxidized product

may be attributed to diffusion of the compound out of the spectroscopically probed region.

Finally, the experimental spectra of both the reduced and superreduced species match the

predicted spectra calculated by TD-DFT, supporting the assignments as Pt(pop-BF$_2$)$^{5-}$ and Pt(pop-

BF$_2$)$^{6-}$, respectively (Figure 6).[ii]

Figure 5: UV-Vis absorption spectra collected in the course of the second reduction to form
Pt(pop-BF$_2$)$^{6-}$ (left), followed by reoxidation to form Pt(pop-BF$_2$)$^{5-}$ (right).
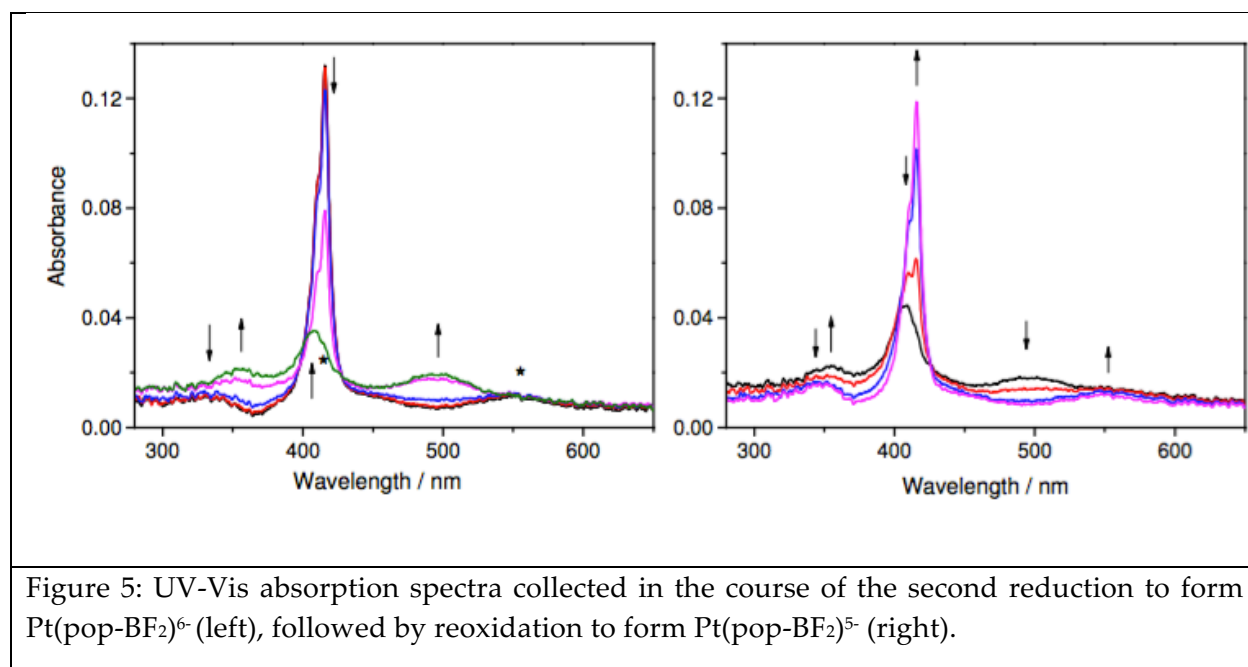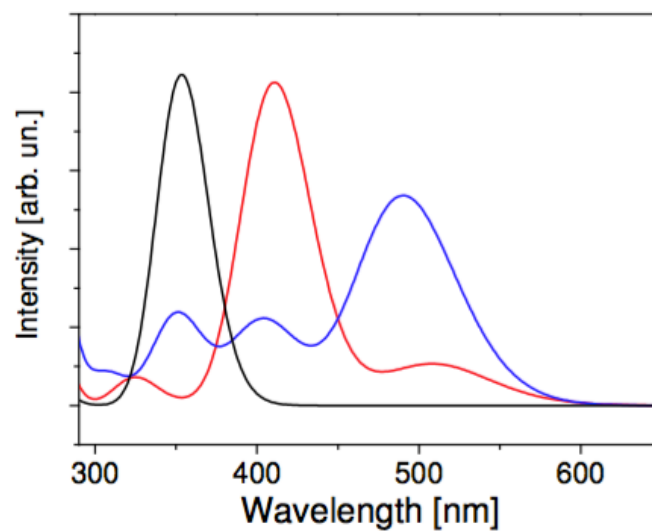
Figure 6: TD-DFT simulated UV-vis absorption spectra of Pt(pop-BF$_2$)$^{n-}$ (n = 4 (black), 5 (red) and 6 (blue). The same FWHM of 3000 cm^{-1} was assumed for all transitions. TD- DFT (PBE0/PCM-MeCN).[ii]

[ii] Theoretical simulations contributed by S. Záliš and A. Vlček.

4.3   Electron paramagnetic resonance (EPR) characterization

In addition to being generated spectroelectrochemically, $Pt(pop-BF_2)^{5-}$ may also be accessed via reduction in acetonitrile with Na/Hg. Reaction of a bright yellow-green acetonitrile solution of $Pt(pop-BF_2)^{4-}$ with Na/Hg affords an immediate color change to a red, which deepens in color over ~ 20 min to form a deep wine-red solution. The EPR spectrum of this solution was measured after freezing to 77 K; the experimental and simulated spectra and fitting parameters are shown

g_1	1.98
g_2	2.03
g_3	2.04
$A_1(Pt)$	900
$A_2(Pt)$	550
$A_3(Pt)$	550
$A_1(Pt')$	900
$A_2(Pt')$	500
$A_3(Pt')$	350

Coupling constants reported in MHz.

Figure 7: Simulated (top) and experimental (bottom) EPR spectra of $Pt(pop-BF_2)^{5-}$ and simulation parameters.
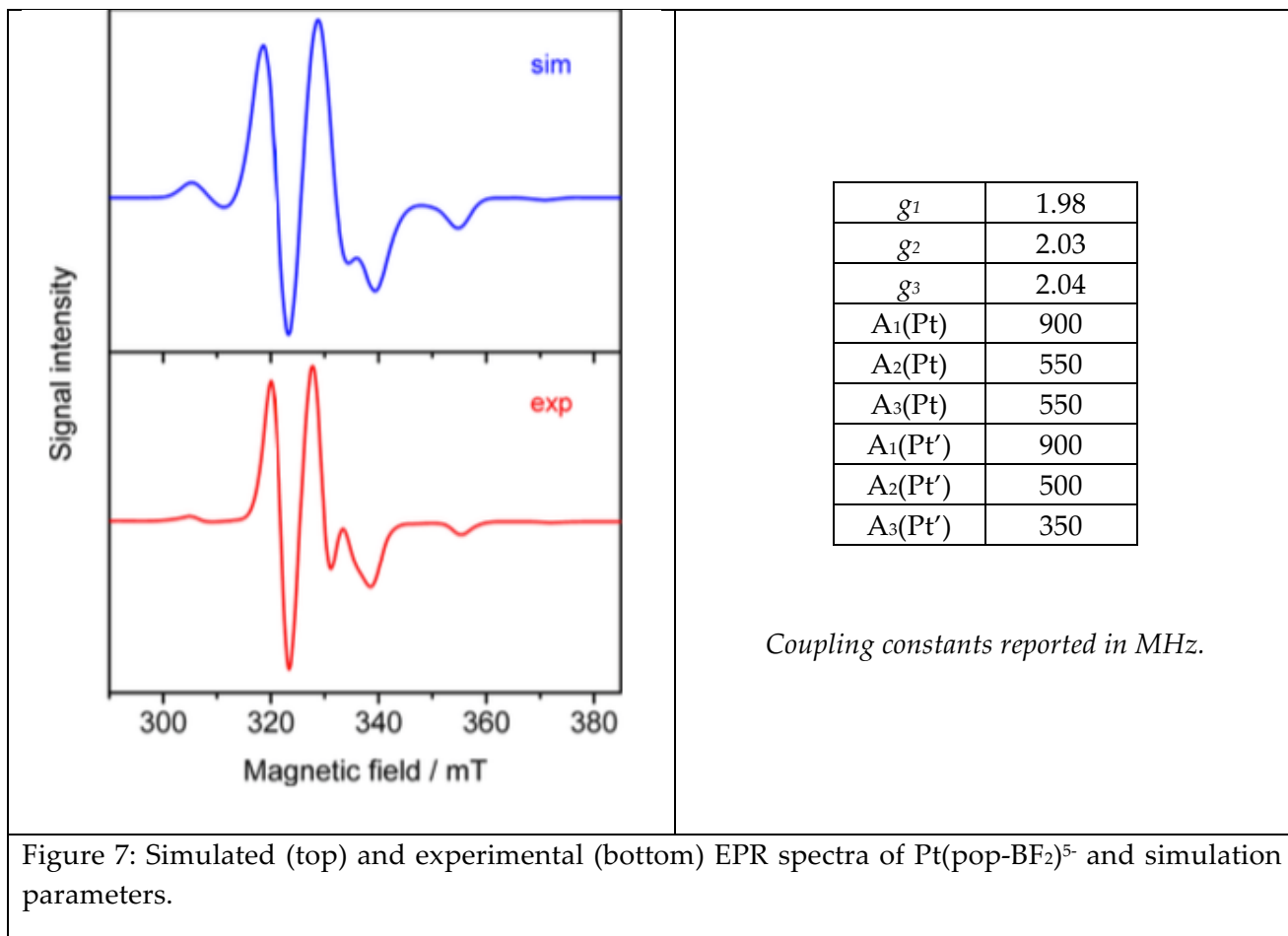
in Figure 7. The spectrum is characteristic of a spin-doublet state with an axial spin distribution ($g_2 \cong g_3 \neq g_1$). The hyperfine splitting constants due to the two ^{195}Pt nuclei are similar, indicating a nearly symmetrical spin density. Finally, the g values are similar to those previously reported for Pt(II) complexes with radical-anion ligands.[11,12] This contrasts with "platinum blue"-type species

in which the unpaired electron is delocalized over four Pt atoms in a molecular orbital with predominantly $5d$ character; such compounds also exhibit axial EPR spectra, but with much larger g values in addition to pronounced anisotropy.[13,14] Finally, still larger g values have been reported Pt^I d^9 sites.[15] This suggests that the unpaired electron in Pt(pop-BF$_2$)$^{5-}$ is delocalized over the two Pt atoms and the ligands in a molecular orbital of $6p$ character.

At room temperature, the EPR-active red solution containing Pt(pop-BF$_2$)$^{5-}$ decomposes over the course of ~24 hours; the solution turns purple and then brown and the intensity of the EPR signal decreases to a fraction of its original value (Figure *8*). Efforts to isolate Pt(pop-BF$_2$)$^{5-}$ chemically were unsuccessful, instead yielding yellow-green Pt(pop-BF$_2$)$^{4-}$ crystals from a red or purple supernatant under a variety of reaction conditions.
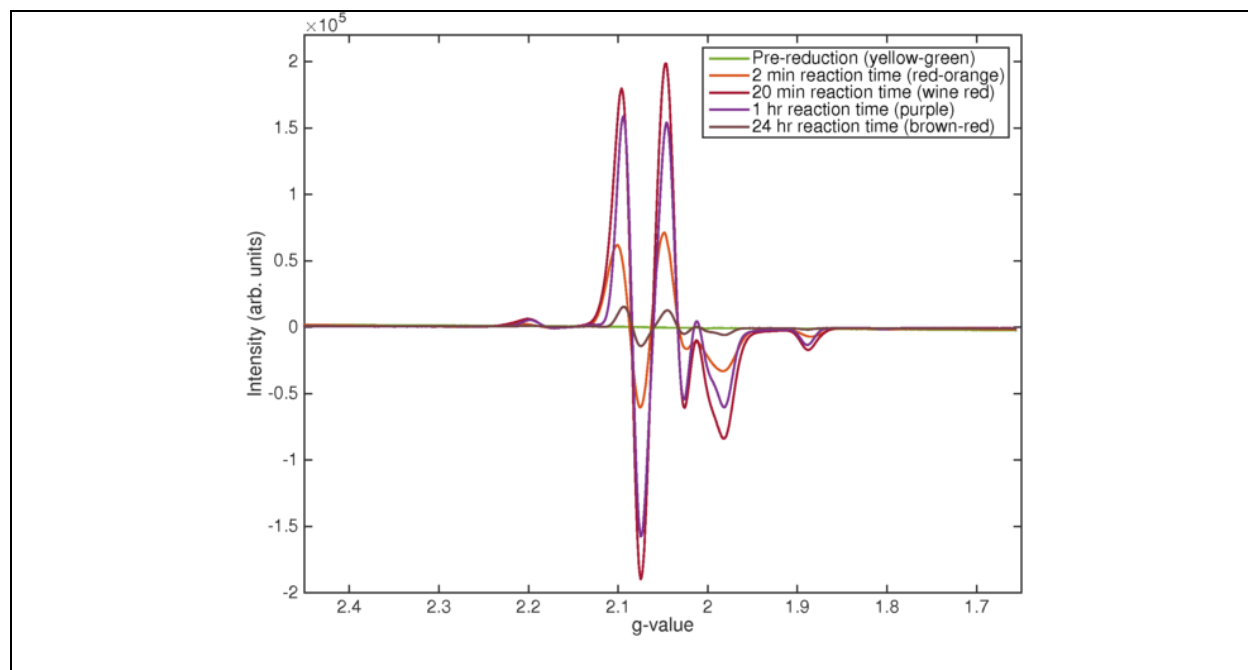
Figure 8: Chemical reduction of Pt(pop-BF$_2$)$^{4-}$ with Na/Hg monitored by EPR over a 24-hour period.

4.4 Electronic structures

The spectroscopic changes recorded in the course of the reduction together with DFT calculations point to successive filling of the pσ molecular orbital. The strong, sharp dσ*→pσ band is the lowest-energy feature in the spectrum of the parent complex. It also is present in the reduced (5-) species with a $(d\sigma^*)^2(p\sigma)^1$ configuration, but it is preceded in energy by a weaker band attributable to pσ excitation. The UV−vis spectral pattern changes completely in the superreduced complex, as the pσ orbital becomes fully occupied. The dσ*→pσ transition vanishes, and the spectrum exhibits a series of transitions from the pσ HOMO to higher unoccupied orbitals.

Successive filling of the pσ orbital formally generates a Pt−Pt σ bond without changing the Pt $5d^8$ electronic configuration, making $Pt(\text{pop-BF}_2)^{6-}$ a very rare $6p^2$ σ-bonded binuclear complex. The DFT-calculated Mayer−Mulliken bond orders[iii] show strengthening of the Pt−Pt bonding interaction upon reduction, whereby the bond order increases about 2-fold on going from the 4− parent (0.17) to the 6− superreduced complex (0.34).[9] While significant, the Pt−Pt bonding in $Pt(\text{pop-BF}_2)^{6-}$ is far from a full σ-bond, as the Pt−Pt bonding interaction is limited by several structural and electronic factors. The rigid pop-BF2 ligand cage does not allow the metal−metal distance to shorten very much, disfavoring effective orbital overlap; the $(5d\sigma)^2(5d\sigma^*)^2(6p\sigma)^2$ configuration places six σ electrons in spatial proximity with one another, producing repulsive electronic congestion along the Pt−Pt axis; and the pσ molecular orbital is only 59% $6p_z$ in character, being delocalized over the Pt−P bonds. Accordingly, Pt−P bond orders

---

[iii] Theoretical simulations contributed by S. Záliš and A. Vlček; further details available in reference 9.

also gradually increase upon reduction. The EPR spectrum of $Pt(pop-BF_2)^{5-}$ confirms the delocalized nature of the singly occupied $6p\sigma$ molecular orbital, showing axial spin density distribution (see section 4.3).

The Pt–Pt distance was calculated to shorten by 0.08 and 0.06 Å upon the first and second reductions, respectively, while the calculated Pt–Pt stretching frequency ν(Pt–Pt) increases from 128 cm^{-1} in the parent complex to 146 (5–) and 170 cm^{-1} (6–).[9] The reduced species essentially keeps the high symmetry of the parent complex, which is manifested both by the calculation and by the EPR spectrum. The most stable conformer of $Pt(pop-BF_2)^{6-}$ shows a small asymmetry, both between the two Pt centers and within each PtP_4 unit, where one pair of trans Pt–P bonds is shorter than the other. The HOMO also is distributed slightly asymmetrically, perhaps due to the "frustrated" $p\sigma$ interaction mentioned above. Nevertheless, the calculated natural charges at the two Pt atoms differ by only 0.035 e^-, in accordance with the $(5d\sigma)^2(5d\sigma^*)^2(6p\sigma)^2$ configuration. This behavior contrasts with that of doubly reduced $5d^8$-$5d^8$ $Ir_2(dimen)_4^{2+}$ (dimen =1,8-diisocyano-p-menthane) that adopts a d^8–d^{10} (Ir^{II}–Ir^0) mixed-valence configuration. In this case, one iridium center maintains a square planar local geometry, while the other distorts toward tetrahedral.[16] Such a distortion avoids the congested $(5d\sigma)^2(5d\sigma^*)^2(6p\sigma)^2$ electronic structure, and its stabilizing effect is manifested by the much smaller difference between the first and second reduction potentials of $Ir_2(dimen)_4^{2+}$ (0.19 V), as compared to $Pt(pop-BF_2)$ (~0.7 V). Such a distortion toward a mixed-valence structure is possible in the $Ir_2(dimen)_4^{2+}$ case because of the

structural flexibility of the dimen bridge,[17] whereas the rigid pop-BF$_2$ ligand cage of Pt(pop-BF$_2$)$^{6-}$ enforces a nearly symmetrical structure, producing the unusual partial 6pσ metal–metal bond.

4.5   Materials and methods

Unless otherwise noted, all reagents were obtained from Sigma-Aldrich and used without further purification; all water used was deionized. All manipulations involving Pt(pop-BF$_2$) were carried out with standard air-free techniques in an inert-atmosphere glovebox or utilizing a vacuum manifold. Solvents were dried using activated alumina columns according to Grubbs' method.[18] Anhydrous acetonitrile (Fisher) was stored over activated 3 Å molecular sieves; all other anhydrous solvents were stored over activated 4 Å molecular sieves.[19] Molecular sieves were activated by heating to 200 °C under reduced pressure for 4 hours.

4.5.1   Electrochemical experiments

All electrochemical experiments were performed with a CH Instruments model 650A electrochemical analyzer. Bu$_4$NPF$_6$ (Fluka) was used as received. Electrolyte solutions were prepared and stored over activated alumina and 4 Å molecular sieves. Cyclic voltammetry (CV) at ambient temperature was measured in a three-electrode configuration consisting of a highly polished glassy-carbon-disk working electrode (A = 0.07 cm^2), a Pt wire auxiliary electrode, and a 1.0 M KCl AgCl/Ag reference electrode, separated by a modified Luggin capillary. Low temperature CV was carried out using a nonisothermal cell configuration, in which the reference electrode was held at ambient temperature, separated from the working compartment by a long glass tube filled with electrolyte, and connected by a Luggin capillary. The temperature was

monitored by a thermocouple placed in the working compartment. The ferrocenium/ferrocene couple has $E^{0\prime} = 0.434$ V, measured at identical experimental conditions.

4.5.2   *Spectroelectrochemical experiments*

Thin-layer spectroelectrochemistry was carried out in a specular-reflectance mode using a modified IR cell. An Ocean Optics UV−vis light source (DH-2000) and spectrometer (USB2000) were connected to the Y-arms of a bifurcated fiber-optic cable; the end of the cable was connected through a lens housing containing a semispherical collimating lens to the front-face window of the spectroelectrochemical cell at a 90° angle. A drop of mineral oil between the fiber optic and front-face quartz window of the cell ensured refractive-index matching. Spectra were not corrected for front-face reflection. The error in intensity at an absorbance of 0.5 is less than 1%. The glassy- carbon working electrode of the spectroelectrochemical cell was attached with silver epoxy to a brass cooling tube, connected to a circulating variable-temperature bath.

4.5.3   *EPR experiments*

EPR spectra were recorded on a Bruker EMS spectrometer at 9.39 GHz. Samples at ~10 mM concentration were prepared by reduction with Na/Hg in dry acetonitrile under an N_2 atmosphere and frozen with liquid nitrogen prior to the measurements. Spectral simulations were performed with MATLAB using the EasySpin MATLAB toolbox (version 4.5.5). Simulation parameters obtained include: g = [2.04, 2.03,1.98]; HStrain=[180,120,100]MHz; A_{Pt1}=[550,550,900] MHz; A_{Pt2} = [350, 500, 900] MHz.

REFERENCES

(1)   Roundhill, D. M.; Gray, H. B.; Che, C. M. *Acc. Chem. Res.* **1989**, *22*, 55.

(2)   Che, C. M.; Butler, L. G.; Gray, H. B.; Crooks, R. M.; Woodruff, W. H. *J. Am. Chem. Soc.* **1983**, *105*, 5492.

(3)   van der Veen, R. M.; Milne, C. J.; El Nahhas, A.; Lima, F. A.; Pham, V. T.; Best, J.; Weinstein, J. A.; Borca, C. N.; Abela, R.; Bressler, C.; Chergui, M. *Angew. Chem., Int. Ed.* **2009**, *48*, 2711.

(4)   Christensen, M.; Haldrup, K.; Bechgaard, K.; Feidenhans'l, R.; Kong, Q.; Cammarata, M.; Russo, M. L.; Wulff, M.; Harrit, N.; Nielsen, M. M. *J. Am. Chem. Soc.* **2008**, *131*, 502.

(5)   Záliš, S.; Lam, Y.-C.; Gray, H. B.; Vlček, A. *Inorg. Chem.* **2015**, *54*, 3491.

(6)   Bryan, S. A.; Schmehl, R. H.; Roundhill, D. M. *J. Am. Chem. Soc.* **1986**, *108*, 5408.

(7)   Che, C. M.; Atherton, S. J.; Butler, L. G.; Gray, H. B. *J. Am. Chem. Soc.* **1984**, *106*, 5143.

(8)   Heuer, W. B.; Totten, M. D.; Rodman, G. S.; Hebert, E. J.; Tracy, H. J.; Nagle, J. K. *J. Am. Chem. Soc.* **1984**, *106*, 1163.

(9)   Darnton, T. V.; Hunter, B. M.; Hill, M. G.; Záliš, S.; Vlček, A.; Gray, H. B. *J. Am. Chem. Soc.* **2016**, *138*, 5699.

(10)   Hofbeck, T.; Lam, Y. C.; Kalbáč, M.; Záliš, S.; Vlček, A.; Yersin, H. *Inorg. Chem.* **2016**, *55*, 2441.

(11)   Braterman, P. S.; Song, J. I.; Wimmer, F. M.; Wimmer, S.; Kaim, W.; Klein, A.; Peacock, R. D. *Inorg. Chem.* **1992**, *31*, 5084.

(12)   Braterman, P. S.; Song, J. I.; Vogler, C.; Kaim, W. *Inorg. Chem.* **1992**, *31*, 222.

(13)   Matsunami, J.; Urata, H.; Matsumoto, K. *Inorg. Chem.* **1995**, *34*, 202.

(14)   Hirani, B.; Li, J.; Djurovich, P. I.; Yousufuddin, M.; Oxgaard, J.; Persson, P.; Wilson, S. R.; Bau, R.; Goddard, W. A.; Thompson, M. E. *Inorg. Chem.* **2007**, *46*, 3865.

(15)   Schmauke, T.; Einar Möller, E.; Roduner, E. *Chem. Commun.* **1998**, 2589.

(16)   Hill, M. G.; Sykes, A. G.; Mann, K. R. *Inorg. Chem.* **1993**, *32*, 783.

(17)   Hunter, B. M.; Villahermosa, R. M.; Exstrom, C. L.; Hill, M. G.; Mann, K. R.; Gray, H. B. *Inorg. Chem.* **2012**, *51*, 6898.

(18)   Pangborn, A. B.; Giardello, M. A.; Grubbs, R. H.; Rosen, R. K.; Timmers, F. J. *Organometallics* **1996**, *15*, 1518.

(19)   Armarego, W. L. F.; Chai, C. L. L. In *Purification of Laboratory Chemicals (Sixth Edition)*; Butterworth-Heinemann: Oxford, 2009, p 88.